Corrosion Science 196 (2022) 109939

Contents lists available at ScienceDirect

Corrosion Science

journal homepage: www.elsevier.com/locate/corsci

Corrosion inhibitors: physisorbed or chemisorbed?

Anton Kokalj [1]

Department of Physical and Organic Chemistry, Jožef Stefan Institute, Jamova 39, SI-1000 Ljubljana, Slovenia

ARTICLE INFO

Keywords:
A. Aluminum
A. Copper
B. Modeling studies
C. Interfaces
C. Neutral inhibition
C. Acid inhibition

ABSTRACT

Adsorption mode of corrosion inhibitors is often determined by criteria based on the standard free energy of adsorption, with values greater than −20 kJ/mol attributed to physisorption and values smaller than −40 kJ/mol attributed to chemisorption. Several arguments are presented herein to show that these are not very reliable criteria to distinguish between physisorption and chemisorption. The most notable among them is that chemisorption may involve bond-breaking and bond-making that result in a rather "weak" standard adsorption free energy (or enthalpy). For this reason, more reliable criteria are recommended that are readily available in first-principle computational modeling studies. The strong molecule–surface interaction, involved in chemisorption, should also be detectable by spectroscopy.

1. Introduction

It is commonly accepted that molecular adsorption is required to achieve corrosion inhibition. This premise was succinctly described by Bockris as *molecule must adsorb to become inhibitor* [1]. A survey of corrosion inhibitor literature further reveals that also a question of whether investigated corrosion inhibitors physisorb or chemisorb is of high interest. To this end, many corrosion inhibitor studies utilize the following criteria based on the standard free energy of adsorption ($\Delta G^{\circ}_{\mathrm{ads}}$) to distinguish between physisorption and chemisorption [2–28]: (i) physisorption: $\Delta G^{\circ}_{\mathrm{ads}} > -20$ kJ/mol, (ii) mixed physisorption/chemisorption: $\Delta G^{\circ}_{\mathrm{ads}} \in [-20, -40]$ kJ/mol, and (iii) chemisorption: $\Delta G^{\circ}_{\mathrm{ads}} < -40$ kJ/mol. For ease of discussion, these criteria will be nicknamed as 20/40 criteria in the following. These criteria are obviously based on the fundamental premise that the chemisorption interaction is strong and the physisorption interaction is weak. To whom the 20/40 criteria can originally be attributed seems rather difficult to determine, because many studies that utilize them cite some previous work that cites some previous work, etc. However, in some studies the works of Donahue and Nobe [29] and Khamis et al. [30] are cited. While the paper of Donahue and Nobe does not contain any reference to these criteria, in the paper of Khamis et al. the 20/40 criteria are established in an empirical way by observing that organic inhibitors in aqueous media usually have the magnitude of the standard free energy of adsorption in the range from 20 to 40 kJ/mol. They attributed the lower end of this range to physisorption and the magnitudes beyond 40 kJ/mol to chemisorption.

The purpose of this article is to show that due to several reasons described herein, the standard free energy of adsorption may not be a reliable criterion to distinguish between physisorption and chemisorption. These reasons were shortly underlined in the previous publication [31], but herein they are elaborated.

2. Arguments against the 20/40 criteria

The problem of using the 20/40 criteria to distinguish between physisorption and chemisorption emerges on two levels: the first is related to issues of how the standard free energies of adsorption are usually determined in experiments and to accompanying uncertainties, whereas the second level is more fundamental, because even when $\Delta G^{\circ}_{\mathrm{ads}}$ is reliably determined it may still not be a reliable criterion to distinguish between physisorption and chemisorption.

E-mail address: tone.kokalj@ijs.si.
[1] URL: http://www.ijs.si/ijsw/K3-en/Kokalj; ORCID ID: 0000-0001-7237-0041

https://doi.org/10.1016/j.corsci.2021.109939
Received 13 August 2021; Received in revised form 3 November 2021; Accepted 5 November 2021
Available online 14 November 2021

As for the first level, related to experimental uncertainties, a common practice to determine the standard Gibbs free energy of adsorption is to utilize the assumption that the experimentally determined inhibition efficiency (IE) is synonymous with the fractional surface coverage (Θ) of adsorbed inhibitor.[2] The standard Gibbs free energy of adsorption is then estimated from the so obtained surface coverage by an adsorption isotherm approach (e.g., Langmuir adsorption isotherm is frequently utilized). However, Lindsay et al. [32] recently argued that the IE = Θ assumption is not necessarily valid and, consequently, that the accuracy of $\Delta G^{\circ}_{\mathrm{ads}}$ so obtained is doubtful.

As for the second level, there are several fundamental reasons why $\Delta G^{\circ}_{\mathrm{ads}}$, even if reliably determined, may not be a reliable criterion to distinguish between physisorption and chemisorption. Here four such arguments are presented.

(i) The first argument is related to the observation that the adsorption enthalpy is a better measure of the adsorption bond strength than the standard adsorption free energy, because the latter involves also entropy contributions [33]. Adsorption is usually characterized by the net loss of roto-translational degrees of freedom and, consequently, the entropy typically decreases during adsorption. In such cases, the standard adsorption free energies are less exergonic (exothermic) than the adsorption enthalpies. In this sense the 20/40 magnitudes seem better suited to adsorption free energies as these were used in the 20/40 criteria postulation [30], whereas the magnitudes for adsorption enthalpy should be correspondingly more exothermic. Along this line of reasoning the criteria based on adsorption enthalpy would differ from those based on standard adsorption free energy only in different threshold values. However, this is certainly an oversimplification, because it will be shown below that the entropy contribution to adsorption can differ considerably between various adsorption modes, which implies that criteria based on the adsorption enthalpy would be more directly related to the adsorption bond strength.

(ii) The second argument is that physisorption is weak only for small molecules, whereas for large molecules it may become stronger than chemisorption [34]. The rationale behind this claim is that chemical interactions, involved in chemisorption, are short ranged and directional, hence a chemisorbed molecule forms one or at most a few chemical bonds with the surface. In contrast, physisorption energy[3] scales with the size of the molecule [35,36], because van der Waals interactions are long ranged and non-directional, hence a large molecule forms many weak physisorption interactions with the surface. Consequently, physisorption can become stronger than chemisorption for large enough molecules [34]. It can be reasoned, though, that this argument is probably more applicable to adsorption at a vacuum/solid interface than at a liquid/solid interface, because at the latter interface the molecule must displace solvent molecules from the surface, whereas at the vacuum/solid interface no such displacement is needed, hence there is no penalty for the molecule to maximize its contact area with the surface.

(iii) The third argument is related to activated adsorption that involves an energy barrier, where the formed molecule–surface bond can be much stronger than the net adsorption enthalpy. Dissociative adsorption is a typical case of activated adsorption, although dissociative adsorption can also be barrierless on reactive surfaces. Due to intramolecular bond-breaking the magnitude of dissociative adsorption enthalpy can be much smaller than the strength of the formed molecule–surface chemical bond. In such cases, the resulting modest adsorption enthalpy would be mistakenly attributed to physisorption. Furthermore, due to the interplay between bond-breaking and bond-making the chemisorption enthalpy can even be endothermic, but the standard adsorption free energy can still be exergonic on behalf of the entropy increase during adsorption, for example, due to desolvation effects, such as the (partial) destruction of ordered solvation shell around the molecule during adsorption. The first part of this argument about endothermic chemisorption is complementary to that of Durnie et al. [37], according to whom an endothermic adsorption is unequivocally a chemisorption, because physisorption is inherently exothermic as it is analogous to fusion (condensation) of a liquid (gas).

(iv) Another argument why chemisorption can result in a modest adsorption enthalpy is related to large adsorbate distortions during chemisorption that are energetically costly [38].

The above stated arguments question the 20/40 criteria from different perspectives. The first argument says that entropy contributions mask the actual molecule–surface bond strength, whereas according to reasons (ii)–(iv) even the adsorption enthalpy may in some cases be unreliable to distinguish between physisorption and chemisorption, because according to reason (ii) also physisorption can be strong, whereas according to reasons (iii) and (iv) chemisorption can result in a modest magnitude of adsorption enthalpy.

These arguments therefore imply that neither the standard free energy of adsorption nor the adsorption enthalpy are reliable criteria to differentiate between physisorption and chemisorption. What, then, are the appropriate criteria to distinguish between physisorption and chemisorption? To try to answer this question, let us first review the definition of physisorption and chemisorption. According to IUPAC, chemisorption involves chemical bond formation [39,40], whereas physisorption involves intermolecular van der Waals forces, which do not involve a significant change in the electronic orbital patterns of the species involved [39,41]. The definition on Wikipedia is also useful: *physisorption is a process in which the electronic structure of the atom or molecule is barely perturbed upon adsorption* [42]. These definitions imply that much more reliable criteria than adsorption energy are readily available in computational studies, such as the molecule–surface bond lengths and the electronic structure analysis of the molecule–surface bonding. Furthermore, the strong molecule–surface bond strength involved in chemisorption should leave signatures detectable experimentally by spectroscopy. For chemisorption the molecule–surface bond length should be compatible with the sum of the covalent radii of the atoms involved in a chemical bond, whereas for physisorption the molecule–surface distance should be similar to the sum of the respective van der Waals radii [43,44]. Electronic structure tools, such as the molecule–surface electron density difference, are also useful to distinguish the two modes of adsorption, because they clearly show the formed molecule–surface bond(s) in the case of chemisorption and almost no perturbation of the electronic structure for physisorption [43,45,46].

3. Results and discussion

To backup the aforementioned arguments that question the 20/40 criteria, three examples based on density-functional-theory (DFT) calculations are provided below with complexity increasing from the first to the last example. The first example considers the gas-phase molecular adsorption on bare metal surfaces, while the second example considers a hydroxylated oxide surface instead. Finally, the third example considers the aqueous-phase molecular adsorption on a hydroxylated metal-oxide surface. The term gas-phase adsorption refers to adsorption at the solid/vacuum interface, whereas the term aqueous-phase adsorption refers to

[2] The relation that IE ≈ Θ stems from the assumption that corrosion rate is proportional to the exposed area of the sample. In such a case the corrosion rate of the uninhibited sample (r_0) is proportional to the area of the sample A, whereas the corrosion rate of the inhibited sample (r) is proportional to the uncovered area of the sample $(1-\Theta)A$, where Θ is a fractional surface coverage of the inhibitor. By utilizing the $r_0 \propto A$ and $r \propto (1-\Theta)A$ relations, it follows straightforwardly that $\mathrm{IE} = \frac{r_0 - r}{r_0} \approx \frac{A-(1-\Theta)A}{A} = \Theta$.

[3] The terms energy (E) and enthalpy (H) are used interchangeably herein, because the difference between the two, $H = E + pV$, is small at ambient conditions. Within the ideal gas approximation, $pV = RT = 2.5$ kJ/mol at 298 K, where R is the universal gas constant. For condensed systems at ambient pressures the pV term is even considerably smaller.

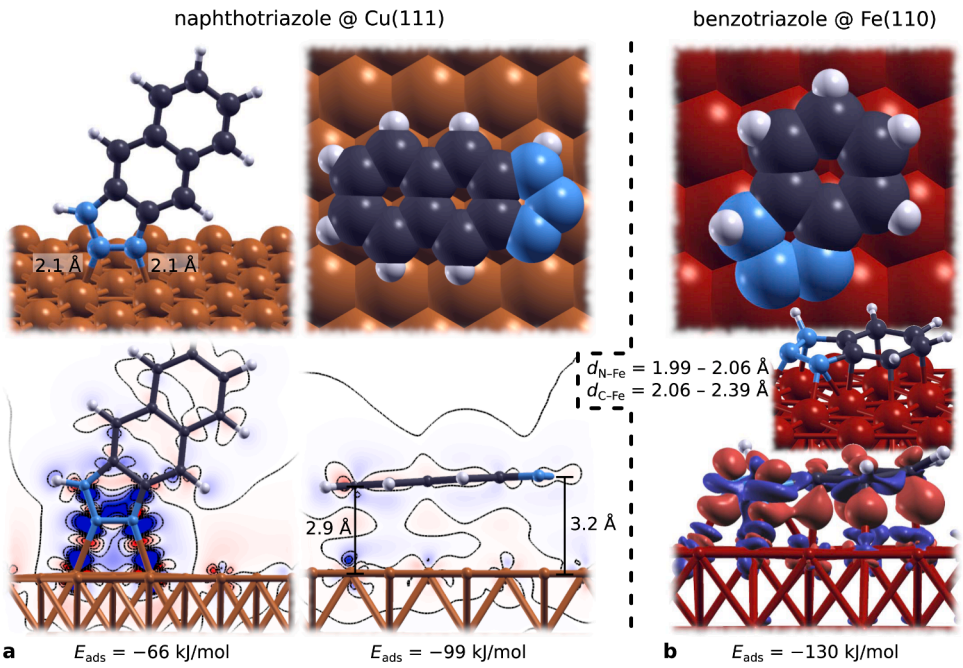

Fig. 1. (a) Weak chemisorption (left) versus physisorption (middle) of naphthotriazole on Cu(111) and (b) benzotriazole chemisorbed parallel onto Fe(110). Top row shows the DFT calculated relaxed structures, whereas bottom row visualizes the molecule–surface electron charge density differences, $\Delta\rho(\boldsymbol{r}) = \rho_{mol/surf}(\boldsymbol{r}) - \rho_{mol}(\boldsymbol{r}) - \rho_{surf}(\boldsymbol{r})$, where the subscripts mol/surf, mol, and surf stand for the molecule/surface, standalone molecule, and bare surface, respectively. In (a) the contours are drawn in the linear scale from −0.006 to +0.006 e/Bohr^3 with the increment of 0.002 e/Bohr^3, whereas in (b) the isosurfaces of ±0.006 e/Bohr^3 are shown. The blue (red) color represents the electron deficient (excess) regions, i.e., the electron charge moved from blue to red regions. Molecule–surface distances and adsorption energies are also given. Note that in (b) the molecule–surface interaction is so strong as to induce the sp^2 to sp^3 rehybridization of the molecular electronic structure as evidenced by the H atoms shifted above the plane of molecular heterocycle. Based on data from Refs. [46, 47].

molecular adsorption from the aqueous-phase onto the solid/liquid-water interface. While for the first example the adsorption is analyzed by the molecule–surface adsorption binding energies, calculated at zero temperature, a full thermodynamic characterization in terms of adsorption enthalpies and standard Gibbs free energies of adsorption is performed for the last two examples. Computational details and the method used to calculate standard adsorption free energies are explained in Appendix A.

3.1. Example 1: gas-phase adsorption on bare metal surfaces

The first example, which is the simplest, shows how the bond distance and electronic structure tools can be utilized to distinguish between chemisorption and physisorption. To this end, Fig. 1a presents the upright and parallel adsorption modes of naphthotriazole on Cu(111) [46]. In the upright adsorption mode, the molecule forms two N–Cu bonds, about 2.1 Å long, which is close to the sum of the involved covalent radii ($r^{N}_{cov} + r^{Cu}_{cov} = 0.71 + 1.32 = 2.03$ Å [48]). The molecule–surface electron charge density difference clearly shows the two formed N–Cu bonds. Note the significant charge redistribution in between the N–Cu atoms with the red-colored electron charge accumulation in the midst of the N–Cu bonds and the blue-colored charge deficit around the involved N and Cu atoms, indicating that the charge moved from the N and Cu atoms toward the bond centers. Both molecule–surface bond lengths and electron charge density difference plot therefore clearly reveal that this adsorption mode can be characterized as weak chemisorption. In contrast, in the parallel adsorption mode the molecule is located about 3 Å above the surface, which is a distance similar to the sum of the involved van der Waals radii ($r^{N}_{vdw} + r^{Cu}_{vdw} = 1.55 + 1.4 = 2.95$ Å and $r^{C}_{vdw} + r^{Cu}_{vdw} = 1.70 + 1.4 = 3.1$ Å [49]), and the electron charge density difference reveals almost no electron charge redistribution, hence both of these criteria reveal that this is physisorption. Interestingly, though, the physisorbed molecule adsorbs stronger ($E_{ads} = -99$ kJ/mol) than the chemisorbed one ($E_{ads} = -66$ kJ/mol). Even if we take into account that DFT may make significant error in estimating the adsorption energy, the difference between the two modes (about 30 kJ/mol) is large enough that it is safe to claim that the two modes are at least comparable in stability. This demonstrates that adsorption energy (enthalpy) may not be a reliable criterion to distinguish between physisorption and chemisorption.

While in the example of Fig. 1a, the upright adsorbed geometry corresponds to weak chemisorption and parallel adsorbed geometry to physisorption, it is not always the case that the parallel adsorption mode corresponds to physisorption. This is demonstrated by Fig. 1b, which shows a benzotriazole molecule adsorbed parallel onto Fe(110) [47]. Note that both the molecule–surface bond-distances of about 2 Å and the large perturbation of electronic structure, visualized by the molecule–surface electron charge density difference, straightforwardly reveal that the molecule is chemisorbed.

It is worth commenting that the large perturbation of the electronic structure due to adsorption of benzotriazole on Fe(110) indicates that the molecule–surface interaction is much stronger than suggested by the net adsorption energy of −130 kJ/mol (Fig. 1b). Indeed, this interaction is so strong as to induce the sp^2 to sp^3 rehybridization of the molecular electronic structure as evidenced by the H atoms shifted above the plane of the molecular heterocycle (Fig. 1b) [47]. A simple analysis in terms of the rigid binding energy,[4] confirms this proposition as it gives 303 kJ/mol for the gross molecule–surface bond strength. The reason for the much smaller magnitude of the adsorption energy of 130 kJ/mol, reported in Fig. 1b, is mainly due to the large molecular deformation upon

[4] The rigid binding energy was calculated as:

$$E^{rigid}_{b} = E_{mol/surf} - E^{rigid}_{mol} - E^{rigid}_{slab},$$

where $E_{mol/surf}$ is the total energy of the relaxed molecule/surface system, whereas E^{rigid}_{mol} and E^{rigid}_{slab} are the total energies of the molecule and the slab, respectively, having the same geometry as in the relaxed molecule/surface system.

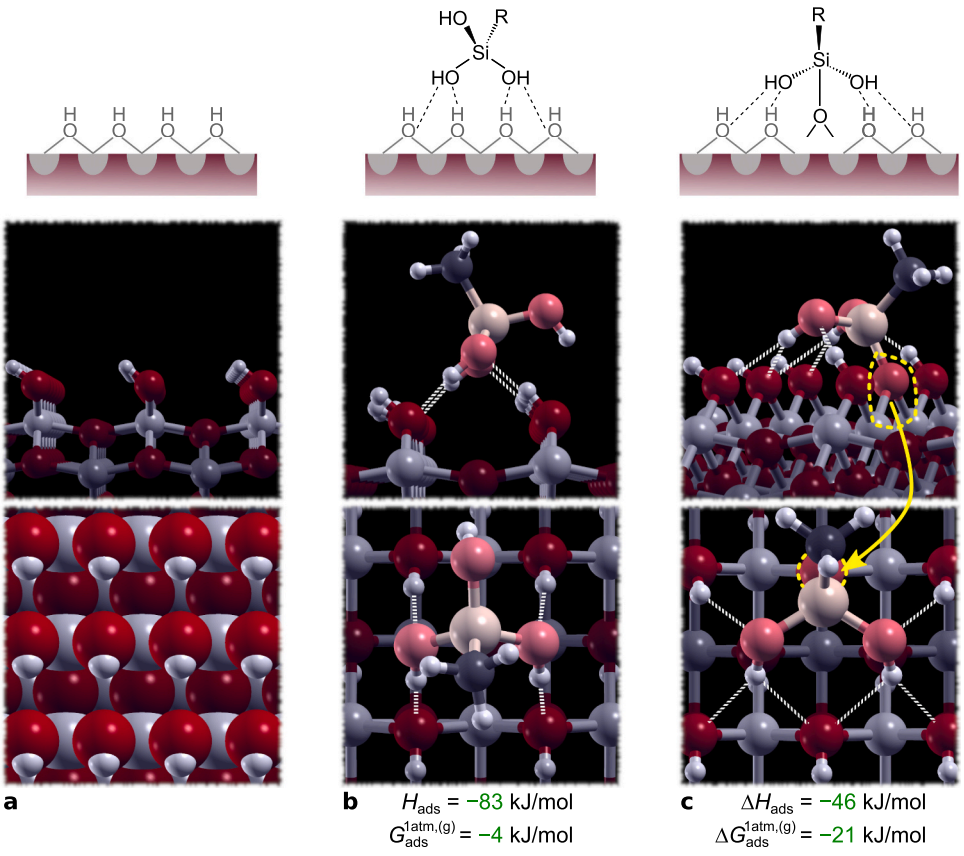

Fig. 2. Top- and side-view snapshots of (a) the boehmite γ-AlOOH(010) surface and the most stable identified (b) plain-adsorption and (c) condensation-adsorption structures of the silanol molecule thereon. The calculated adsorption (reaction) enthalpies and the standard Gibbs free energies at $T = 298.15$ K and $p = 1$ atm are also given (for definition of $G^{1atm,(g)}_{ads}$ and $\Delta G^{1atm,(g)}_{ads}$, see Appendix A.3). In (c) the silanol's O atom that is involved in the SiO–Al bonding is encircled with dashed yellow. Color coding of atoms: H = small white balls, C = black, O = reddish, Al = gray (topmost Al ions are colored brighter). Based on Refs. [51,52].

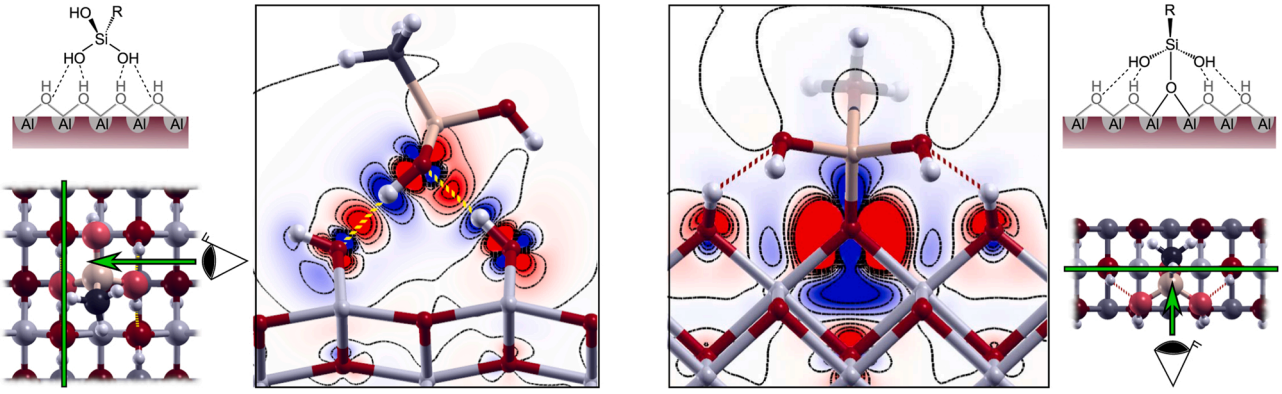

Fig. 3. Silanol–surface electron charge density difference, $\Delta\rho(\boldsymbol{r}) = \rho_{mol/surf}(\boldsymbol{r}) - \rho_{mol}(\boldsymbol{r}) - \rho_{surf}(\boldsymbol{r})$, for plain-adsorption (left) and condensation-adsorption (right) on γ-AlOOH(010). The contours are drawn in linear scale from −0.006 to +0.006 e/Bohr^3 with the increment of 0.002 e/Bohr^3. Schematic representation of the adsorbed structures as well as the planes of the contour plots are also shown on the far left and far right. For plain-adsorption (left) the contour plane coincides with the plane of the two H-bonds. For condensation adsorption (right) the contour plane coincides with the plane of the bifurcated molecule–surface O–Al bond, whereas H-bonds are outside the shown plane.

adsorption, which costs 159 kJ/mol,[5] whereas the deformation of the substrate costs only 14 kJ/mol. This corroborates the fourth argument stated in Section 2, which claims that chemisorption can result in a modest adsorption enthalpy due to large adsorbate distortions during adsorption that are energetically costly.

Although the examples of Fig. 1 corroborate the arguments (ii) and (iv) presented in Section 2, these examples are only toy models in the context of corrosion, because in real environments metal surfaces are not clean but are instead covered with a native oxide-layer and, possibly, an outer layer of (oxy)hydroxide or other precipitated corrosion products. Nevertheless, these examples confirm, at least conceptually, that arguments (ii) and (iv) are sound.

3.2. Examples 2 and 3: gas-phase and aqueous-phase adsorption on oxidized surfaces

As to corroborate the arguments that question the 20/40 criteria also by examples that are more relevant for corrosion, oxidized surfaces are

[5] The cost of molecular deformation upon adsorption was calculated as:

$$E^{deformation}_{mol} = E^{rigid}_{mol} - E_{mol},$$

where E_{mol} is the total energy of the relaxed standalone molecule and E^{rigid}_{mol} is the total energy of the molecule having the same geometry as in the adsorbed state.

considered by the next two examples. To this end, the adsorption of methylsilanetriol, $CH_3Si(OH)_3$, on oxidized Al surfaces is considered [50–52]. Here $CH_3Si(OH)_3$ is used as a model silanol molecule. In the previous publication [51], the adsorption of this molecule was studied on four chemically and structurally diverse surface models of hydroxylated oxidized Al surface as to account for the fact that the structure of the oxidized aluminum surface is not uniquely determined, i.e., it is presumably non-crystalline and varies depending on the method of preparation [53,54]. For the sake of simplicity, only two out of the four surface models are considered herein, in particular, boehmite γ-AlOOH (010) and hydroxylated α-Al_2O_3(001); for description of the two surface models, see Appendix A.

Taking into account the molecular structure of $CH_3Si(OH)_3$ and the fully hydroxylated nature of the two surface models, two different adsorption modes can be envisaged. The first is the plain adsorption mode, where the molecule adsorbs on the surface by forming intermolecular H-bonds between its OH groups and surface OH groups. The corresponding adsorption reaction can be as written:

$$\mathrm{MolH} + * \rightarrow \mathrm{MolH}^*, \tag{1}$$

where the label MolH designates an intact molecule, * stands for the free adsorption site, and MolH* for the adsorbed molecule. This adsorption mode is referred to as the plain adsorption, because it does not involve any bond-breaking. The second viable adsorption mode follows the condensation mechanism that involves bond-breaking and bond-making, where the silanol molecule forms a strong SiO–Al chemical bond with the surface by replacing a surface OH group by transforming it into a water molecule, i.e.:

$$\mathrm{MolH} + \mathrm{OH}^* \rightarrow \mathrm{Mol}^* + \mathrm{H_2O}, \tag{2}$$

where OH* stands for the surface hydroxyl group and Mol* for the adsorbed deprotonated molecule (note the omitted H).

The snapshots of the most stable identified structures for the two adsorption modes of silanol molecule on the boehmite γ-AlOOH(010) surface are shown in Fig. 2. In the plain adsorption mode (Fig. 2b), the silanol molecule forms four H-bonds with the surface OH groups (the molecule is twice H-bond donor and twice H-bond acceptor) and the corresponding adsorption enthalpy and standard free energy are −83 kJ/mol and −4 kJ/mol, respectively, calculated at a temperature of 298.15 K and a partial pressure of 1 atm. The average H-bond strength, derived from the adsorption enthalpy, is therefore about 20 kJ/mol.

In the condensation adsorption mode (Fig. 2c), the molecule forms a strong bifurcated SiO–Al bond, i.e., the pertinent O atom is located on the bridge site and bonds to two surface Al ions. In addition, the molecule forms four H-bonds with the surface OH groups, two of them being bifurcated. Interestingly, despite the formation of the strong bifurcated SiO–Al chemical bond and the four H-bonds, the adsorption enthalpy of −46 kJ/mol is by about 40 kJ/mol less exothermic than the one of the plain adsorption. That the bifurcated SiO–Al chemical bond is much stronger than the H-bonds between the molecule and the surface is confirmed by the electron charge density difference (Fig. 3). Note the much stronger electron charge redistribution around the bifurcated SiO–Al bond compared to that involved in the H-bonds.[6] The reason that a much stronger molecule–surface interaction results in a less exothermic adsorption enthalpy is due to bond-breaking. In particular, during the condensation adsorption two chemical bonds are broken (SiO–H and Al–OH) and two new chemical bonds are formed (SiO–Al and H–OH); in addition, the intermolecular H-bonds are also formed. In this case, the adsorption enthalpy corresponds to the difference between the strengths of the broken and formed bonds and therefore provides no direct information about the strength of the molecule–surface interaction.[7] This is the principle reason why adsorption enthalpy (or standard adsorption free energy) is not a reliable criterion to distinguish between physisorption and chemisorption or, more generally, between weaker and stronger molecule–surface interaction. This example, therefore, corroborates the third argument presented in Section 2.

Fig. 2 further reveals that the calculated standard adsorption free energies are less exergonic (exothermic) than adsorption enthalpies. The reason is the loss of roto-translational degrees of freedom during adsorption.[8] For the $CH_3Si(OH)_3$ molecule, the roto-translational contributions to the free energy at $T = 298.15$ K and $p = 1$ atm amount to −75 kJ/mol, whereas for plain adsorption the difference between the standard adsorption enthalpy and free energy is −79 kJ/mol (Fig. 2b) thus confirming that the difference is by and large due to the loss of roto-translational degrees of freedom upon adsorption.

While the adsorption enthalpy of plain adsorption mode is significantly more exothermic than that of the condensation adsorption mode, the opposite is true for the standard adsorption free energy (cf. Figs. 2b and 2c). The reason that the standard adsorption free energy of condensation adsorption mode is more exergonic than that of the plain adsorption mode can again be attributed to the roto-translational degrees of freedom, because a water molecule is released during condensation adsorption. The roto-translational contributions to the free energy of H_2O at $T = 298.15$ K and $p = 1$ atm amount to −49 kJ/mol. Hence, the net difference between the loss and gain of roto-translational degrees of freedom during condensation adsorption is $75 - 49 = 26$ kJ/mol, which

[6] The electron charge density difference of the plain-adsorption mode (Fig. 3) clearly shows the formed H-bonds between the molecular and the surface OH groups. Indeed, it is a well known fact that, in addition to electrostatic attraction, strong H-bonds also have some features of covalent bonding. Molecules adsorbed via strong H-bonds can be therefore considered as a borderline between physisorption and weak-chemisorption (note the much stronger perturbation of the electronic structure compared to that of physisorbed naphthotriazole on Cu(111), shown in Fig. 1a). However, whether the molecule is physisorbed or chemisorbed is not really the main point in this example, but rather that weaker molecule–surface bonding can result in a more exothermic adsorption enthalpy than stronger molecule–surface bonding.

[7] The strength of the formed SiO–Al molecule–surface bond can be estimated with aid of additional auxiliary calculations. In particular, the adsorption energy can be written as the difference between the broken and formed bonds, i.e.:

$$\Delta E_{\mathrm{ads}} = \sum_i^{N_{\mathrm{broken}}} D_i - \sum_j^{N_{\mathrm{formed}}} D_j,$$

where D_i (or D_j) stands for a given bond strength; note that bond strengths are positive by convention. By plugging in the respective components, we have:

$$\Delta E_{\mathrm{ads}} = (D_{\mathrm{Al-OH}} + D_{\mathrm{SiO-H}}) - (D_{\mathrm{Al-OSi}} + D_{\mathrm{H-OH}} + D_{\mathrm{H-bonds}}),$$

hence:

$$D_{\mathrm{Al-OSi}} = (D_{\mathrm{Al-OH}} + D_{\mathrm{SiO-H}}) - (D_{\mathrm{H-OH}} + D_{\mathrm{H-bonds}} + \Delta E_{\mathrm{ads}}).$$

Alternatively, the total molecule–surface interaction strength ($D_{\mathrm{Al-OSi}} + D_{\mathrm{H\text{-}bonds}}$) can be estimated by desorbing the molecule via the homolytic cleavage of the SiO–Al bond. Hence:

$$D_{\mathrm{Al-OSi}} + D_{\mathrm{H-bonds}} = E_{\mathrm{Mol\cdot}} + E_{\mathrm{surf\cdot}} - E_{\mathrm{Mol/surf}},$$

where $E_{\mathrm{Mol/surf}}$ is the total energy of the adsorption system, $E_{\mathrm{Mol\cdot}}$ is the total energy of the isolated $CH_3Si(OH)_2O\cdot$ radical, and $E_{\mathrm{surf\cdot}}$ is the total energy of the surface having an OH vacancy (note that during condensation adsorption a molecule substitutes one OH group and this vacancy corresponds to it). The respective calculations give the value of 606 kJ/mol for the strength of the total molecule–surface interaction ($D_{\mathrm{Al-OSi}} + D_{\mathrm{H\text{-}bonds}}$). By estimating the $D_{\mathrm{H\text{-}bonds}}$ component from the adsorption enthalpy of the plain adsorption mode, the corresponding value for the $D_{\mathrm{Al-OSi}}$ is about 520 kJ/mol, which indeed confirms that the SiO–Al chemical bond is very strong.

[8] According to author's experience, the vibrational contributions to reaction free energy for the adsorption of organic molecules on oxidized Al surfaces usually largely cancel out between products and reactants, thus being typically within ±20 kJ/mol [55].

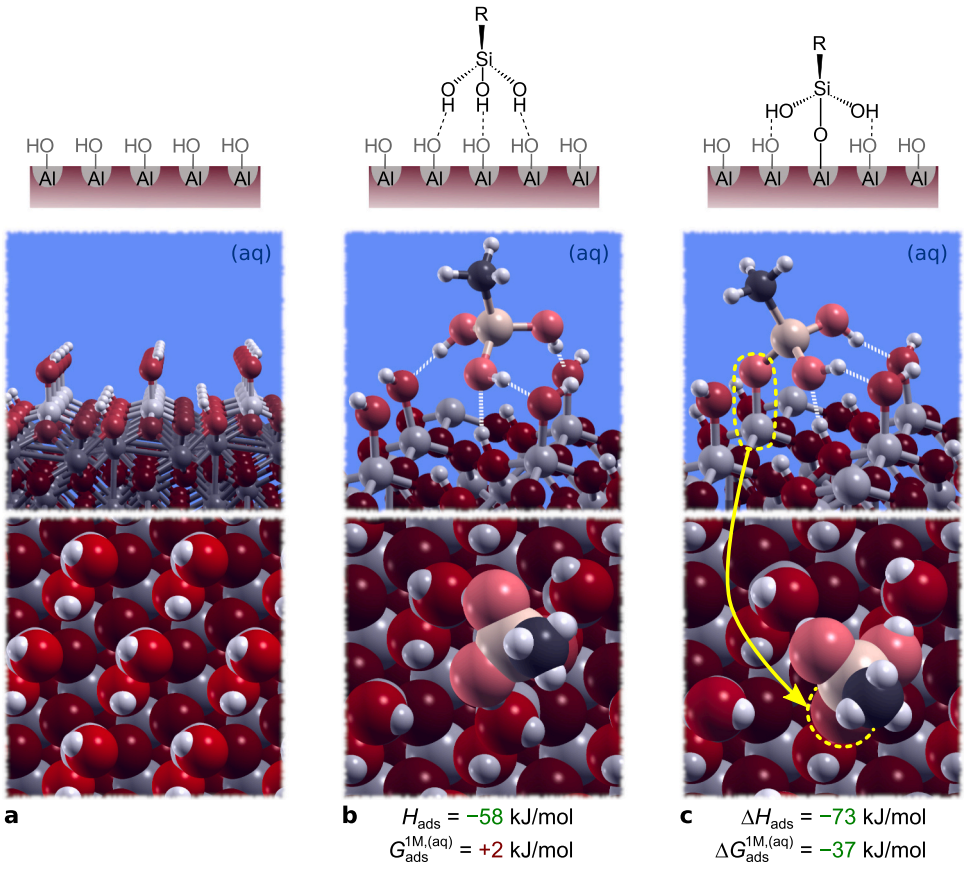

Fig. 4. Similar to Fig. 2, but for aqueous-phase adsorption of the silanol molecule on the hydroxylated α-Al_2O_3(001) surface. The calculated adsorption (reaction) enthalpies and the standard Gibbs free energies at $T = 298.15$ K and $c = 1$ M are also given (for definition of $G^{1M,(aq)}_{ads}$ and $\Delta G^{1M,(aq)}_{ads}$, see Appendix A.3). In (c) the silanol's O atom that is involved in the SiO–Al bonding is encircled with dashed yellow.

is very close to the difference between the $\Delta G^{1atm,(g)}_{ads}$ and ΔH_{ads} of 25 kJ/mol (Fig. 2c), where the labels $\Delta G^{1atm,(g)}_{ads}$ and ΔH_{ads} stand for the standard adsorption free energy and adsorption enthalpy, respectively (see Appendix A.3). This implies that in this case the difference between $\Delta G^{1atm,(g)}_{ads}$ and ΔH_{ads} is almost exclusively due to roto-translational contributions. This example thus corroborates the first argument presented in Section 2, in particular that entropy contributions can mask the actual molecule–surface bond strength (note that the largest contribution to the roto-translational free energy is due to the entropy $-TS$ term).[9]

It is worth noting from Fig. 2 that the entropy contributions to the standard adsorption free energy differ considerably between plain and condensation adsorption, because for plain adsorption the TS contribution[10] amounts to 79 kJ/mol at $T = 298.15$ K and $p = 1$ atm, whereas for condensation adsorption it amounts to 25 kJ/mol. This corroborates the statement made in Section 2 that the entropy contribution to adsorption can differ considerably between various adsorption modes.

While on the boehmite γ-AlOOH(010) surface model (Fig. 2), the adsorption enthalpy of plain adsorption mode is more exothermic than that of condensation adsorption, the opposite is true on hydroxylated α-Al_2O_3(001), where condensation adsorption is more exothermic than plain adsorption (Fig. 4). The data presented in Fig. 4 correspond to aqueous-phase adsorption, but the trend is preserved also if the adsorption at a solid/vacuum interface is considered instead (Table 1). The two examples, presented in Figs. 2 and 4, reveal that stronger molecule–surface bonding may or may not result in more exothermic adsorption enthalpy and, consequently, that the adsorption enthalpy is not a reliable criterion to distinguish between weak and strong molecule–surface bonding and, in turn, between physisorption and chemisorption. Although for both presented cases, the standard free energy of adsorption is more exergonic for condensation adsorption (strong molecule–surface bonding) than for plain adsorption (weak molecule–surface bonding), this does not yet make the standard adsorption free energy a reliable criterion to distinguish between the physisorption and chemisorption. Note that the calculated standard free energy of condensation adsorption of silanol on boehmite γ-AlOOH(010) is only −21 kJ/mol that according to the 20/40 criteria would be mostly attributed to physisorption, which is not the case. Furthermore, an important factor that makes the silanol standard adsorption free energy of the condensation adsorption more exergonic than that of the plain adsorption is the release of a water molecule and the corresponding gain of the roto-translational degrees of freedom, which has nothing to do with the molecule–surface bond-strength.

3.2.1. *Gas-phase vs. aqueous-phase adsorption*

Table 1 summarizes the gas-phase and aqueous-phase adsorption

[9] The roto-translational (rt) Gibbs free energy can be written as $G_{rt} = E_{rt} + pV - TS_{tr}$, where E_{rt} is the roto-translational thermal energy. For a non-linear molecule, the roto-translational thermal energy is $3RT$, which with the pV term sums to $4RT = 10$ kJ/mol at 298.15 K (here the ideal gas $pV = RT$ relation was used). For condensation adsorption the $4RT$ contribution cancels out due to the release of a water molecule.

[10] The entropy contribution (TS) is obtained from the fundamental thermodynamic relation, $G = H - TS$, and the data presented in Fig. 2.

Table 1
Gas-phase and aqueous-phase adsorption energies, enthalpies, and standard Gibbs free energies for plain and condensation adsorption of the $CH_3Si(OH)_3$ molecule on γ-AlOOH(010) and hydroxylated α-Al_2O_3(001). For plain adsorption the tabulated adsorption quantities are labeled as X_{ads}, cf. Eq. (A.9), and for condensation-adsorption as ΔX_{ads}, cf. (A.10). E_{ads} and ΔE_{ads} values are calculated from the Kohn-Sham total energies calculated at 0 K without the zero-point-energy (ZPE) correction, i.e., E_0 of Eq. (A.1). In contrast, E°_{ads} and ΔE°_{ads} are calculated from the $E(T)$ values of Eq. (A.1) with ZPE included and H°_{ads} and ΔH°_{ads} are calculated from the $H(T)$ values of Eq. (A.4) at $T = 298.15$ K. Standard adsorption free energies G°_{ads} and ΔG°_{ads} are calculated at $T = 298.15$ K and either $p = 1$ atm (gas-phase) or $c = 1$ M (aqueous-phase). G°_{ads} and ΔG°_{ads}correspond to $G^{1atm,(g)}_{ads}$ and $\Delta G^{1atm,(g)}_{ads}$ for gas-phase adsorption and to $G^{1M,(aq)}_{ads}$ and $\Delta G^{1M,(aq)}_{ads}$ for aqueous-phase adsorption, as defined in Appendix A.3.

	plain adsorption				condensation adsorption			
	MolH + * → MolH*				MolH + OH* → Mol* + H_2O			
	E_{ads} (kJ/mol)	E°_{ads} (kJ/mol)	H°_{ads} (kJ/mol)	G°_{ads} (kJ/mol)	ΔE_{ads} (kJ/mol)	ΔE°_{ads} (kJ/mol)	ΔH°_{ads} (kJ/mol)	ΔG°_{ads} (kJ/mol)
γ-AlOOH(010)								
gas-phase	−96	−81	−83	−4	−48	−46	−46	−21
aqueous-phase	−69	−54	−56	+16	−28	−27	−27	+8
hydroxylated α-Al_2O_3(001)								
gas-phase	−95	−86	−89	−20	−90	−91	−91	−66
aqueous-phase	−65	−56	−58	+2	−71	−73	−73	−37

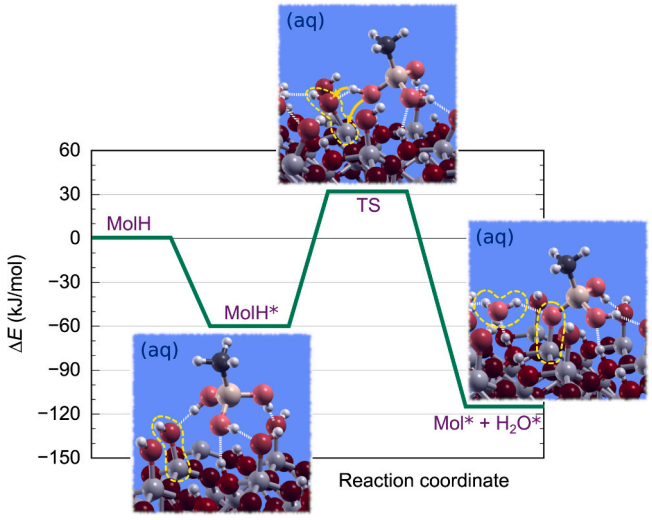

Fig. 5. Schematized reaction energy profile for aqueous-phase adsorption of the silanol molecule on hydroxylated α-Al_2O_3(001) as going from solvated molecule (MolH) to plain adsorption mode (MolH*) and then passing the transition state (TS) to reach the condensation adsorption mode with the co-adsorbed water molecule (Mol* + H_2O*). In the MolH* and TS snapshots the OH* group that transforms to H_2O* is encircled. In the TS snapshot the arrows indicate the motion of the proton to form the H_2O molecule and the motion of the O atom to form the SiO–Al bond, whereas in the Mol* + H_2O* snapshot the water molecule and the silanol–surface SiO–Al chemical bond are encircled. Reaction energy profile consists of Kohn-Sham energies, calculated at 0 K without the zero point energy corrections, i.e., E_0 in Eq. (A.1). The reference zero energy corresponds to solvated silanol molecule. The calculated energy barrier for the MolH* → Mol* + H_2O* elementary reaction step is 92 kJ/mol.

energies, enthalpies, and standard free energies for the two examples of Figs. 2 and 4. It is worth noting that the aqueous-phase values are consistently less exothermic (exergonic) than the gas-phase values. This is not surprising and can be attributed, in part, to the cost of (partial) desolvation of a molecule during adsorption. Furthermore, the molecule must also displace water molecule(s) from the surface as to make place for itself.

Table 1 further reveals that condensation adsorption is more exothermic (exergonic) on hydroxylated α-Al_2O_3(001) than on boehmite γ-AlOOH(010). The condensation reaction on the former surface involves the transformation of μ_1-OH into H_2O, whereas the reaction on the latter surface involves the transformation of μ_2-OH.[11] This result is therefore in line with the observation that the μ_1-OH groups are usually more basic than the μ_2-OH groups [56,57].

3.2.2. *Activation barrier of condensation adsorption*

According to the Gibbs free energy criterion, condensation adsorption of silanol on the two surface models of hydroxylated oxidized Al surface (Figs. 2 and 4) is predicted to be thermodynamically preferred over plain adsorption. However, condensation adsorption involves bond-breaking, hence to observe such adsorption experimentally (at a given temperature), the activation energy for bond-breaking should not be too high. For this reason, the activation energy barrier for the condensation adsorption was calculated by modeling the transformation from the plain to the condensation adsorption mode by the following elementary reaction step:

$$\mathrm{MolH^* + OH^* \rightarrow Mol^* + H_2O^*}, \quad (3)$$

which involves the shift of a proton from the silanol OH group to the surface OH group (as to form a water molecule) and the formation of an

[11] The difference between μ_1-OH and μ_2-OH is that the former is bonded to one and the latter to two surface Al ions.

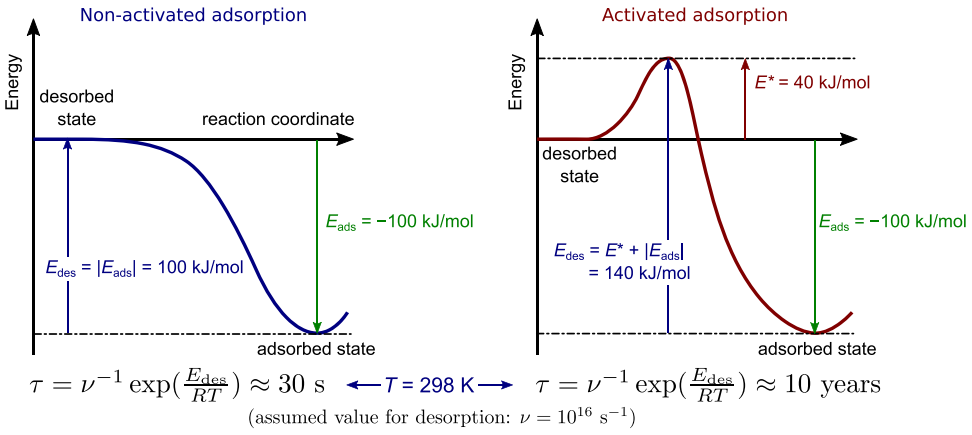

Fig. 6. The difference between non-activated and activated adsorption for the persistence of the adsorbed molecule on the surface. For both cases the adsorption energy of 100 kJ/mol is considered and the activation barrier of 40 kJ/mol is assumed for activated adsorption. A typical residence time of an adsorbed molecule on the surface can be estimated from the inverted Arrhenius equation, $\tau = \nu^{-1}\exp(E_{des}/RT)$, where E_{des} is the desorption energy, R is the universal gas constant, and the value of $\nu = 10^{16}$ s^{-1} is assumed for the frequency prefactor of desorption [58, 59]. At room temperature, the quoted parameter values lead to typical residence times of a molecule on the surface of about 30 seconds for non-activated adsorption and about 10 years for activated adsorption.

SiO–Al chemical bond with the surface. This reaction step can be seen as the second elementary step in the overall condensation adsorption reaction, i.e., (i) MolH → MolH*, (ii) MolH* + OH* → Mol* + H_2O*, (iii) Mol* + H_2O* → Mol* + H_2O. The calculated activation barrier for reaction (3) is 92 kJ/mol, which implies that it is feasible at room temperature.[12] The corresponding transition-state structure along with the schematic reaction energy profile is shown in Fig. 5.

The drawback of the current activation energy calculation is that the aqueous solvent is considered only implicitly, hence it cannot capture the indirect Grotthuss-like proton transfer that is assisted by water molecules via the concerted motion of protons through the hydrogen bond network. Such indirect proton transfer may display a lower activation barrier than direct one, as indirect proton transfers were observed in the transformation of surface hydroxyl groups into water molecules on oxidized Al surfaces [57].

3.3. Non-activated vs. activated adsorption

Let us also comment on an interesting issue associated with activated adsorption and corrosion inhibition. As mentioned in Introduction, it is commonly accepted that molecular adsorption is required to achieve corrosion inhibition. This premise implies that an efficient inhibitor should persist on the surface. A typical residence time of an adsorbed inhibitor molecule on the surface depends exponentially on the desorption energy, i.e., the higher is the desorption energy, the longer is the residence time of an adsorbed inhibitor on the surface. For non-activated adsorption, the desorption energy can be approximated by the magnitude of the adsorption energy, $E_{des} \approx |E_{ads}|$. For activated adsorption, in contrast, the desorption energy is higher than the magnitude of the adsorption energy, because it is given by $E_{des} \approx |E_{ads}| + E^*$, where E^* is the activation barrier for activated adsorption.[13] This implies that for a given value of adsorption energy, the residence time of a molecule on the surface can differ greatly between non-activated and activated adsorption, as schematically illustrated in Fig. 6. The arguments presented on this figure illuminate a widely-known statement that chemisorption is slow and irreversible. It is slow because it is activated and it appears irreversible because the adsorption activation barrier sufficiently increases the desorption energy, which exponentially increases the persistence of the chemisorbed molecule on the surface.

These arguments make desorption energy a much more relevant parameter than adsorption energy for corrosion inhibition, because it is the desorption energy rather than the adsorption energy that determines the persistence of molecules on the surface. Yet, even desorption energy may fail to distinguish between chemisorption and physisorption, particularly with respect to the arguments (ii) and (iv) in Section 2.

3.4. Physisorbed or chemisorbed: does it matter?

In light of the arguments presented herein, what is the point of distinguishing between physisorption and chemisorption then? While the issue of the adsorption type is certainly interesting from an academic point of view, it is instead the persistence of inhibitor molecules on the surface and the stability and impermeability of inhibitor protective layers thereon that matter for corrosion inhibition. Although a strong molecule–surface interaction appears to be useful for inhibiting corrosion, it is a necessary rather than a sufficient condition because it is by no means the only relevant factor for corrosion inhibition. Furthermore, a sound argument can be made that a stronger molecule–surface bonding does not yet entail a better inhibition, because otherwise species such as chloride ions, which interact very strongly with metals [60–62], would act as corrosion inhibitors, yet they activate corrosion instead. In this sense, a corrosion inhibition analogue of the Sabatier principle[14] can be postulated, according to which the inhibitor should adsorb strongly enough to persist on the surface, but not too strongly or else it can promote metal dissolution because too strong molecule–metal interaction can weaken the neighboring lattice metal–metal and/or metal–oxygen bonds [63,64]. The idea behind this premise is schematically presented in Fig. 7. Indeed, a suggestion that a given descriptor of corrosion inhibition may display an optimal range of values is known in the literature [65–67].

4. Conclusions

To summarize, four arguments were presented to demonstrate that the often used so-called 20/40 criteria are not very reliable to

[12] A typical time scale (τ) of an elementary reaction event can be estimated from the inverted Arrhenius equation, $\tau = \nu^{-1}\exp(E^*/RT)$, where E^* is the activation energy and ν is the frequency prefactor. According to transition state theory a typical value for the prefactor ν is 10^{13} s^{-1}. At room temperature this value of ν gives $\tau \approx 20$ min for the reaction with $E^* = 92$ kJ/mol.

[13] Whether adsorption is activated or not can be determined experimentally, for example, by a combination of adsorption calorimetry (as to deduce the adsorption enthalpy) and temperature programmed desorption (as to deduce the desorption energy). For activated adsorption with a sizable barrier, the two values should differ significantly.

[14] Sabatier principle in heterogeneous catalysis states that the best catalyst is neither too mild nor too reactive. A too mild catalyst does not bind reactants, hence reaction cannot take place. In contrast, a too reactive catalyst binds products too strongly, hence they cannot desorb and this in turn inactivates the catalyst.

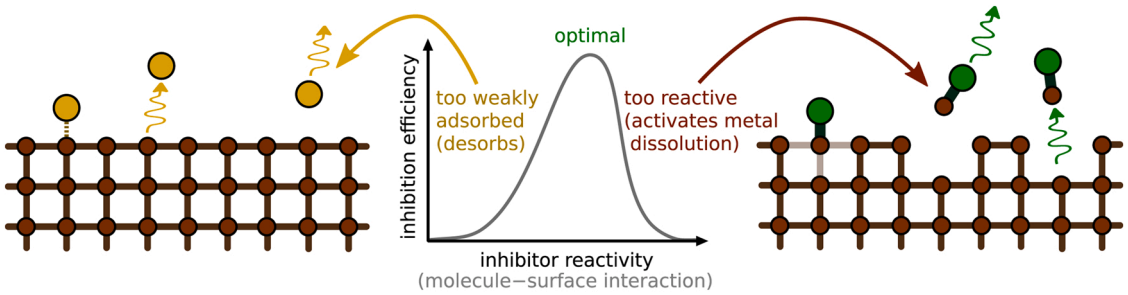

Fig. 7. Schematic illustration of a corrosion inhibition analogue of the Sabatier principle. If the inhibitor–surface interaction is too weak, the inhibitor molecules do not persist on the surface and quickly desorb. In contrast, a too strong inhibitor–surface interaction can weaken the adjacent lattice metal–metal (and/or metal–oxygen) bonds, which makes metal dissolution easier. This suggests that the optimal inhibitor–surface interaction should be therefore neither too weak nor too strong. The shown dependence of the inhibition efficiency on the inhibitor reactivity should be taken only conceptually rather than quantitatively, as it can be reasonably argued that corrosion inhibition is too complex to be described by only a single descriptor.

distinguish between physisorption and chemisorption. These criteria are based on the fundamental fact that the chemisorption interaction is strong and the physisorption interaction is weak, hence values of standard free energy of adsorption above −20 kJ/mol are attributed to physisorption and values below −40 kJ/mol are attributed to chemisorption.

The weakest of the presented arguments against the 20/40 criteria is that the adsorption enthalpy is a better measure of the adsorption bond strength than the standard free energy of adsorption, because for the latter the entropy contributions mask the actual molecule–surface bond strength. The second presented argument questions the 20/40 criteria by observing that physisorption is weak only for small molecules, whereas for large molecules it may become stronger than chemisorption. It can be reasoned, though, that this argument is probably more applicable to adsorption at a gas/solid interface than at a liquid/solid interface. The last two arguments attack the 20/40 criteria by observing that chemisorption can result in a modest magnitude of the adsorption enthalpy due to either bond-breaking or large adsorbate distortions during chemisorption, both of which are energetically costly. In such cases, it is worth noting that chemisorbed molecules can persist on the surface for an extended period of time despite the weak adsorption enthalpy, which results from bond-breaking upon adsorption. If such bond-breaking is characterized by the activation barrier than the desorption energy can be considerably higher than the magnitude of the adsorption enthalpy (this is the origin of the commonly used phrase that chemisorption is slow an irreversible). Desorption energy is therefore much more relevant than adsorption energy for corrosion inhibition, because it is desorption energy that determines the persistence of molecules on the surface.

One should therefore resist to differentiate between physisorption and chemisorption solely on the basis of the standard adsorption free energy, particularly when its value is modest. More reliable criteria are therefore required to distinguish between physisorption and chemisorption. Such criteria are readily available in computational modeling studies, two of them being the molecule–surface distance and the electronic structure analysis of the molecule–surface bonding, whereas experimentally the type of adsorption can be investigated spectroscopically, because the strong molecule–surface interaction involved in chemisorption should leave signatures detectable by spectroscopy.

CRediT authorship contribution statement

Conceptualization, Methodology, Investigation, Formal analysis, Writing - Original Draft, Writing - Reviewing and Editing, Visualization.

Declaration of Competing Interest

The author declares that he has no known competing financial interests or personal relationships that could have appeared to influence the work reported in this paper.

Data Availability

The data presented in this manuscript are based on previous publications [46,47,50,51]. The raw data required to reproduce the example 1 are available to download from an open-source online data repository hosted at Mendeley Data: https://doi.org/10.17632/2v75sp987f.1, whereas the data required to reproduce examples 2 and 3 cannot be shared at this time as the data also form part of an ongoing study.

Acknowledgments

The author thanks Prof. Ingrid Milošev for bringing the subject of corrosion inhibitors to his attention and Dr. Matic Poberžnik for helpful discussions. This work has been financially supported by the Slovenian Research Agency (Grant No. P2-0393).

Appendix A. Computational details

Calculations were performed in the framework of DFT using the generalized gradient approximation of Perdew-Burke-Ernzerhof [68] and the pseudopotential method with ultrasoft pseudopotentials (US-PP) [69,70] as implemented in the PWscf code from the QUANTUM ESPRESSO distribution [71,72].

The examples presented in Section 3 are based on previous publications [46,47,50,51], hence the computational details are kept compatible to the original sources. For adsorption of azoles on Cu and Fe surfaces (Fig. 1), the Kohn-Sham orbitals were expanded in a plane-wave basis set with the kinetic energy cutoff of 30 Ry (240 Ry for the charge density). Cu(111) and Fe(110) surfaces were described with slabs consisting of four atomic layers. The bottom layer was constrained to the bulk positions and the in-plane lattice spacing was fixed to the calculated equilibrium bulk lattice parameter of Cu and Fe. Molecules were adsorbed on one side of the slab and the thickness of the vacuum region—the distance between the top of the ad-molecule and the adjacent slab—was set to more than 10 Å. Brillouin zone integrations were performed with the special point technique [73] using k-meshes of quality compatible to the $8 \times 8 \times 1$ k-mesh of the Cu(111)–(1×1) and Fe(110)–(1×1) unit cells. Fermi surface effects were treated with a

Methfessel-Paxton smearing [74] of 0.03 Ry. For a proper description of the parallel adsorption mode of naphthotriazole on Cu(111), a reparemetrized [46] semi-empirical dispersion correction of Grimme [75] was used.

For adsorption of a silanol $CH_3Si(OH)_3$ molecule on hydroxylated oxidized Al surfaces, two different surface models were utilized, one based on γ-AlOOH(010) and the other on hydroxylated α-Al_2O_3(001). The two surface models have the surface densities of OH groups of 9.3 and 9.4 OH/nm^2, respectively. Kohn-Sham orbitals were expanded in a plane-wave basis set with the kinetic energy cutoff of 35 Ry (280 Ry for the charge density). Molecular adsorption was modeled with the (3 × 3) supercell of γ-AlOOH(010) and the (2 × 2) supercell of α-Al_2O_3(001) using the Γ k-point. Atomic structures of the two surface models are shown in Figs. 2a and 4a, whereas further technical details of the two surface models are described in the previous Ref. [51]. For these calculations, all degrees of freedom were relaxed and vibrational frequencies were calculated at the Γ q-point using the PHonon code [76] from QUANTUM ESPRESSO [71,72]. A quasi harmonic approximation of Cramer-Truhlar [77] was applied, that is, the vibrational frequencies below 100 cm^{-1} were raised to 100 cm^{-1} to remedy the breakdown of the harmonic oscillator model for low-frequency vibrational modes (at room temperature 100 cm^{-1} corresponds to about $RT/2$).

For aqueous-phase adsorption, calculations were performed in the aqueous-phase with the solvent described implicitly using the Environ plugin [78] for QUANTUM ESPRESSO and the soft-sphere-continuum-solvation (SoftCS) implicit-solvent method [79].

Activation energies were calculated with the climbing image nudged elastic band (CI-NEB) method [80,81]. With the NEB method the reaction pathway is modeled as the minimum energy path (MEP) between the reactant (initial state, IS) and the product (final state, FS). The transition state (TS) is the maximum energy configuration on the MEP and the activation energy is calculated as the difference in energy between the TS and IS, $E^* = E_{TS} - E_{IS}$. In CI-NEB calculations, the threshold for the magnitude of the atomic force components was set below 50 meV/Å.

A.1. Thermodynamics equations

The total energy of the investigated system at a given temperature T can be written as:

$$E(T) = E_0 + E_{trv}(T), \tag{A.1}$$

where E_0 designates the Kohn-Sham total energy, calculated at 0 K without the zero point energy (ZPE), and $E_{trv}(T)$ stands for translational + rotational + vibrational thermal energies at temperature T with ZPE included (this notation implies that $E_{trv}(0) = E_{vib}(0) = \text{ZPE}$, where E_{vib} designates vibrational energy). The reason for such a decomposition is that calculating Kohn-Sham total energies at 0 K without ZPE is computationally much easier and less CPU intensive than calculating vibrational frequencies. This implies that adsorption energies can be calculated on two levels of rigor: either from (i) the Kohn-Sham total energies E_0, calculated at 0 K without ZPE (this is straightforward and therefore usually utilized), or from (ii) the energies $E(T)$, calculated at a given temperature T by taking into account also ZPE (this is less straightforward and therefore much less often utilized). The latter requires CPU-intensive vibrational calculations. Note, however, that once the vibrational frequencies are calculated, it is straightforward to access enthalpy and Gibbs free energy, i.e.:

$$H(T,p) = E_0 + E_{trv}(T) + pV \tag{A.2}$$

and

$$G(T,p) = H(T,p) - TS_{trv}(T,p). \tag{A.3}$$

For gaseous species the roto-translational contributions were treated using the rigid-rotor model[15] and the ideal gas approximation ($pV = RT$), hence the enthalpy can be written as:

$$H(T) = E_0 + E_{trv}(T) + RT. \tag{A.4}$$

Within the ideal gas approximation the translational partition function (q_t) and the corresponding entropy (S_t) are:

$$q_t = \left(\frac{mkT}{2\pi\hbar^2}\right)^{\frac{3}{2}} V = \left(\frac{mkT}{2\pi\hbar^2}\right)^{\frac{3}{2}} \frac{kT}{p} \tag{A.5a}$$

and

$$S_t(T,p) = R\left(\ln q_t(T,p) + \frac{5}{2}\right), \tag{A.5b}$$

where m is the mass of a molecule, $\hbar$ is the reduced Planck constant, and k is the Boltzmann constant. The combination of Eqs. (A.3)–(A.5) leads to the well-known equation:

$$G(T,p_1) = G(T,p_0) + RT\ln\frac{p_1}{p_0}. \tag{A.6}$$

For surfaces and adsorbates thereon, only the vibrational contributions to thermal energy and entropy were considered, whereas the

[15] For a non-linear molecule, the rotational partition function is:

$$q_r = \frac{1}{\sigma_{rot}}\cdot\frac{\sqrt{8\pi(kT)^3 I_A I_B I_C}}{\hbar^3},$$

where I_A, I_b, and I_C are the three eigenvalues of the moment of inertia tensor, σ_{rot} is the rotational symmetry number, and $\hbar$ is the reduced Planck constant. The corresponding rotational contributions to thermal energy and entropy are:

$$E_r(T) = \frac{3}{2}RT \quad \text{and} \quad S_r(T) = R\left(\ln q_r(T) + \frac{3}{2}\right).$$

configurational entropy of adsorbates was neglected.[16] The pV term was also neglected, because it is minute for solids.[17] Hence:

$$H(T) \approx E_0 + E_{\mathrm{vib}}(T) \tag{A.7}$$

and

$$G(T) \approx H(T) - TS_{\mathrm{vib}}(T). \tag{A.8}$$

A.2. Standard states

For standard states in the gas-phase, the temperature of 298.15 K and the partial pressure of 1 atm are chosen, whereas in aqueous solution the concentration of 1 M is used. A given thermodynamic quantity X of a molecular species calculated at partial pressure of 1 atm is labeled as X^{1atm}, whereas when calculated at concentration of 1 M (or the corresponding partial pressure) it is labeled as X^{1M}. In contrast to molecular species, the partial pressure is irrelevant for macroscopic bodies (e.g., surfaces) within the current treatment;[18] this is inline with Eq. (A.8), where only vibrational degrees of freedom are considered in the calculation of Gibbs free energy.

A.3. Calculation of standard free energies of adsorption

In the following the term gas-phase adsorption refers to adsorption at the solid/vacuum interface, whereas the term aqueous-phase adsorption refers to molecular adsorption from the aqueous-phase onto the solid/liquid-water interface.

In the gas-phase, the adsorption energy, enthalpy or Gibbs free energy of the plain adsorption mode, reaction (1), is calculated as:

$$X_{\mathrm{ads}} = X_{\mathrm{MolH/surf}} - X_{\mathrm{surf}} - X_{\mathrm{MolH}}, \tag{A.9}$$

where X stands for either E_0, $E(T)$, $H(T)$, or $G(T)$ as defined above and the labels MolH/surf, surf, and MolH stand for the adsorption system, plain surface, and standalone molecule, respectively. The corresponding equation for the condensation adsorption, reaction (2), is:

$$\Delta X_{\mathrm{ads}} = X_{\mathrm{Mol/surf}} + X_{\mathrm{H_2O}} - X_{\mathrm{OH/surf}} - X_{\mathrm{MolH}}, \tag{A.10}$$

where the symbol ΔX_{ads} is used instead of X_{ads}, first, to distinguish the two adsorption energies and, second, to indicate that condensation adsorption is a chemical reaction that involves bond-breaking and bond-making. Note that here $X_{\mathrm{OH/surf}}$ is identical to X_{surf} in Eq. (A.9), but here the prefix OH is added to indicate that one surface OH group is transformed into water during the reaction, hence the surface after condensation adsorption contains one OH group per supercell less than before adsorption.

As for aqueous-phase adsorption, the standard Gibbs free energies of adsorption are calculated by means of a thermodynamic cycle [83]. The utilized thermodynamic cycles for plain and condensation adsorption are presented in Fig. A.8. They combine the gas-phase calculations that give the Gibbs free energies in the gas-phase and the implicit solvent calculations as to obtain the Gibbs free energies of solvation. Namely, a very convenient feature of the implicit solvent calculations is that the Gibbs free energy of solvation (G_{solv}) is readily calculated as the difference between the total energies obtained from the *in solvent* and *in vacuo* calculations:[19]

$$G_{\mathrm{solv}} = E_0^{(\mathrm{aq})} - E_0^{(\mathrm{g})}, \tag{A.11}$$

where $E_0^{(\mathrm{aq})}$ is the Kohn-Sham total energy (calculated at 0 K without ZPE) of the relaxed system in the aqueous-phase and $E_0^{(\mathrm{g})}$ is the analogous total energy of the relaxed system in vacuum (which is taken to represent the gas-phase).

To obtain the standard free energy of a solvated molecular species, one also needs to account for different standard states in the gas-phase (partial pressure of 1 atm) and solution (concentration of 1 M). The free energy of solvated species at 1 M concentration can be thus written as (cf. Fig. A.8):

$$G^{\mathrm{1M,(aq)}} = G^{\mathrm{1atm,(g)}} + RT\ln\frac{\text{“1M”}}{\text{“1atm”}} + G_{\mathrm{solv}} \tag{A.12}$$

where the labels “1M” and “1atm” are symbolic representations of the respective concentrations or partial pressures, which at 298.15 K correspond to:

$$\text{“1atm”} \equiv 1\ \mathrm{atm} \equiv 0.04088\ \mathrm{M}, \tag{A.13}$$

$$\text{“1M”} \equiv 1\ \mathrm{M} \equiv 24.46\ \mathrm{atm}, \tag{A.14}$$

hence at 298.15 K:

$$RT\ln\frac{\text{“1M”}}{\text{“1atm”}} = 8\ \mathrm{kJ/mol}. \tag{A.15}$$

[16] In the Langmuir adsorption model, the chemical potential of an adsorbed species is [82]:

$$\mu_{\mathrm{ads}} = \mu_{\mathrm{ads}}^0 + RT\ln\frac{\Theta}{1-\Theta},$$

where Θ is the fractional surface coverage. This implies that a convenient standard state for adsorbed species is at $\Theta = 1/2$, because the logarithmic term vanishes.

[17] At ambient pressures, the volume of solids is about 1000 times smaller than that of the ideal gas, hence the pV term of solids is on the order of $10^{-3}\ RT$.

[18] In statistical-mechanical sense this implies no translational degrees of freedom for macroscopic bodies, because the dependence of Gibbs free energy on partial pressure comes from translational degrees of freedom, cf. Eq. (A.5), and the pV term that is vanishing for solids at ambient pressures.

[19] The implicit solvent methods are so parametrized that this difference gives the free energy of solvation.

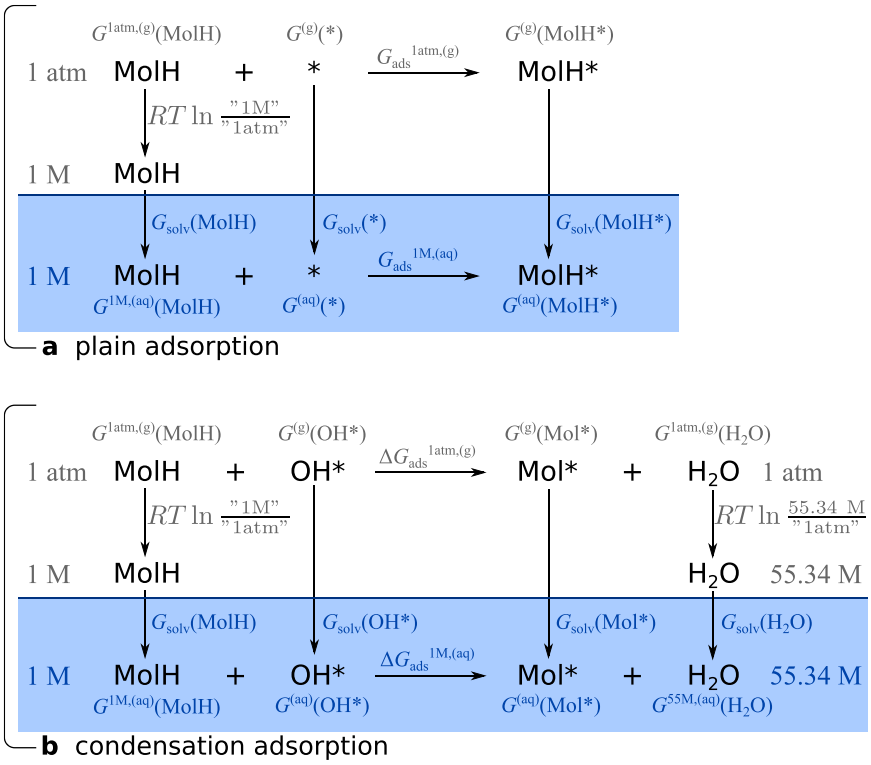

Fig. A.8. Thermodynamics cycles utilized for the calculation of the aqueous-phase standard free energy of adsorption for (a) plain and (b) condensation adsorption.

During condensation adsorption, a water molecule is formed which is then self-solvated in the aqueous solvent. This case requires a special treatment, because the concentration of a liquid water at 298.15 K is 55.34 M.[20] The free energy of a liquid water can thus be written as:

$$G_{H_2O}^{(aq)} = G^{1atm,(g)} + RT\ln\frac{55.34\text{M}}{\text{“1atm”}} + G_{solv}, \tag{A.16}$$

where (cf. Eq. (A.13)):

$$RT\ln\frac{55.34\ \text{M}}{\text{“1atm”}} = 18\ \text{kJ/mol}. \tag{A.17}$$

In contrast to molecular species, the concentration is irrelevant for macroscopic bodies (e.g. surfaces), hence the free energy of solvated bare slabs (and adsorption systems) can be calculated as:

$$G_{slab}^{(aq)} = G_{slab}^{(g)} + G_{solv}. \tag{A.18}$$

With the above definitions and the thermodynamic cycle of Fig. A.8a, the aqueous-phase standard Gibbs free energy of plain adsorption ($G_{ads}^{1M,(aq)}$) can be estimated as:

$$G_{ads}^{1M,(aq)} = G_{ads}^{1atm,(g)} + \Delta G_{solv} - RT\ln\frac{\text{“1M”}}{\text{“1atm”}} = G_{ads}^{1atm,(g)} + \Delta G_{solv} - 0.08\ \text{kJ/mol}, \tag{A.19}$$

where ΔG_{solv} is given by:

$$\Delta G_{solv} = G_{solv}(\text{MolH*}) - G_{solv}(*) - G_{solv}(\text{MolH}), \tag{A.20}$$

and $G_{ads}^{1atm,(g)}$ stands for the gas-phase standard plain adsorption free energy at the molecular partial pressure of 1 atm, i.e.:

$$G_{ads}^{1atm,(g)} = G^{(g)}(\text{MolH*}) - G^{(g)}(*) - G^{1atm,(g)}(\text{MolH}), \tag{A.21}$$

where the labels G(MolH*) and G(*) represent the respective free energy components ($G^{(g)}$ or G_{solv}) of the adsorption system and the bare surface, respectively, hence they are equivalent to $X_{\text{MolH/surf}}$ and X_{surf} in Eq. (A.9).

Analogously, the aqueous-phase standard Gibbs free energy of condensation adsorption ($\Delta G_{ads}^{1M,(aq)}$) can be estimated with aid of the thermodynamic cycle of Fig. A.8b, i.e.:

$$\Delta G_{ads}^{1M,(aq)} = \Delta G_{ads}^{1atm,(g)} + \Delta G_{solv} - RT\ln\frac{\text{“1M”}}{\text{“1atm”}} + RT\ln\frac{55.34\ \text{M}}{\text{“1atm”}} = \Delta G_{ads}^{1atm,(g)} + \Delta G_{solv} + 10\ \text{kJ/mol}, \tag{A.22}$$

[20] This concentration stems from the density of liquid water of 997.048 g/l at 298.15 K [84].

where $\Delta G_{\text{ads}}^{1\text{atm,(g)}}$ stands for the gas-phase condensation adsorption free energy at the molecular partial pressure of 1 atm, i.e.:

$$\Delta G_{\text{ads}}^{1\text{atm,(g)}} = G^{(\text{g})}(\text{Mol*}) + G^{1\text{atm,(g)}}(\text{H}_2\text{O}) - G^{(\text{g})}(\text{OH*}) - G^{1\text{atm,(g)}}(\text{MolH}) \tag{A.23}$$

and ΔG_{solv} is given by:

$$\Delta G_{\text{solv}} = G_{\text{solv}}(\text{Mol*}) + G_{\text{solv}}(\text{H}_2\text{O}) - G_{\text{solv}}(\text{OH*}) - G_{\text{solv}}(\text{MolH}), \tag{A.24}$$

where the labels G(Mol*) and G(OH*) represent the respective free energy components ($G^{(\text{g})}$ or G_{solv}) of the adsorption system and the bare surface, respectively, hence they are equivalent to $X_{\text{Mol/surf}}$ and $X_{\text{OH/surf}}$ in Eq. (A.10).

Finally, let us also consider a bit closer the self-solvation of a water molecule. The respective solvation free energy can be straightforwardly obtained from the water vapor pressure and basic thermodynamics, i.e., at equilibrium the free energies of liquid water and its vapor are equal ($G^{(\text{g})} = G^{(\text{l})} \equiv G_{\text{H}_2\text{O}}^{(\text{aq})}$). The water vapor partial pressure at 298.15 K is 0.0313 atm [84], which leads to the self-solvation free energy of water of −27 kJ/mol,[21] whereas the DFT calculated value, obtained from the currently utilized SoftCS implicit solvent method, is −24 kJ/mol. The DFT calculated value is therefore in good agreement with the value derived from the experimental vapor partial pressure. For consistency reasons with other calculations, the calculated value of −24 kJ/mol was used herein.

References

[1] J.O'M. Bockris, A.K.N. Reddy, Modern electrochemistry, 2nd Edition, vol. 2B, Kluwer Academic/Plenum Publishers, New York, 2000.

[2] M. Scendo, Corrosion inhibition of copper by potassium ethyl xanthate in acidic chloride solutions, Corros. Sci. 47 (11) (2005) 2778–2791, https://doi.org/10.1016/j.corsci.2004.12.001.

[3] I.B. Obot, N.O. Obi-Egbedi, A.O. Eseola, Anticorrosion potential of 2-mesityl-1H-imidazo[4,5-f][1,10]phenanthroline on mild steel in sulfuric acid solution: Experimental and theoretical study, Ind. Eng. Chem. Res. 50 (4) (2011) 2098–2110, https://doi.org/10.1021/ie102034c.

[4] I.B. Obot, N.O. Obi-Egbedi, Adsorption properties and inhibition of mild steel corrosion in sulphuric acid solution by ketoconazole: Experimental and theoretical investigation, Corros. Sci. 52 (1) (2010) 198–204, https://doi.org/10.1016/j.corsci.2009.09.002.

[5] E. Machnikova, K.H. Whitmire, N. Hackerman, Corrosion inhibition of carbon steel in hydrochloric acid by furan derivatives, Electrochim. Acta 53 (20) (2008) 6024–6032, https://doi.org/10.1016/j.electacta.2008.03.021.

[6] F. Bentiss, M. Lebrini, M. Lagrené, Thermodynamic characterization of metal dissolution and inhibitor adsorption processes in mild steel/2,5-bis(*n*-thienyl)-1,3,4-thiadiazoles/hydrochloric acid system, Corros. Sci. 47 (12) (2005) 2915–2931, https://doi.org/10.1016/j.corsci.2005.05.034.

[7] F. Bentiss, M. Lebrini, H. Vezin, F. Chai, M. Traisnel, M. Lagrené, Enhanced corrosion resistance of carbon steel in normal sulfuric acid medium by some macrocyclic polyether compounds containing a 1,3,4-thiadiazole moiety: AC impedance and computational studies, Corros. Sci. 51 (9) (2009) 2165–2173, https://doi.org/10.1016/j.corsci.2009.05.049.

[8] E.E. Ebenso, I.B. Obot, Inhibitive properties, thermodynamic characterization and quantum chemical studies of secnidazole on mild steel corrosion in acidic medium, Int. J. Electrochem. Sci. 5 (12) (2010) 2012–2035.

[9] R. Hasanov, S. Bilge, S. Bilgiç, G. Gece, Z. Kılıç, Experimental and theoretical calculations on corrosion inhibition of steel in 1 M H_2SO_4 by crown type polyethers, Corros. Sci. 52 (3) (2010) 984–990, https://doi.org/10.1016/j.corsci.2009.11.022.

[10] I. Ahamad, R. Prasad, M.A. Quraishi, Inhibition of mild steel corrosion in acid solution by pheniramine drug: Experimental and theoretical study, Corros. Sci. 52 (9) (2010) 3033–3041, https://doi.org/10.1016/j.corsci.2010.05.022.

[11] I. Ahamad, R. Prasad, M.A. Quraishi, Experimental and quantum chemical characterization of the adsorption of some schiff base compounds of phthaloyl thiocarbohydrazide on the mild steel in acid solutions, Mater. Chem. Phys. 124 (2–3) (2010) 1155–1165, https://doi.org/10.1016/j.matchemphys.2010.08.051.

[12] M.A. Hegazy, A.S. El-Tabei, A.H. Bedair, M.A. Sadeq, An investigation of three novel nonionic surfactants as corrosion inhibitor for carbon steel in 0.5 M H_2SO_4, Corros. Sci. 54 (2012) 219–230, https://doi.org/10.1016/j.corsci.2011.09.019.

[13] E. Jamalizadeh, S. Hosseini, A. Jafari, Quantum chemical studies on corrosion inhibition of some lactones on mild steel in acid media, Corros. Sci. 51 (6) (2009) 1428–1435, https://doi.org/10.1016/j.corsci.2009.03.029.

[14] K.F. Khaled, Molecular simulation, quantum chemical calculations and electrochemical studies for inhibition of mild steel by triazoles, Electrochim. Acta 53 (9) (2008) 3484–3492, https://doi.org/10.1016/j.electacta.2007.12.030.

[15] S. Bilgiç, M. Şahin, The corrosion inhibition of austenitic chromium-nickel steel in H_2SO_4 by 2-butyn-1-ol, Mater. Chem. Phys. 70 (3) (2001) 290–295, https://doi.org/10.1016/S0254-0584(00)00534-4.

[16] S. Kumar, D. Sharma, P. Yadav, M. Yadav, Experimental and quantum chemical studies on corrosion inhibition effect of synthesized organic compounds on N80 steel in hydrochloric acid, Ind. Eng. Chem. Res. 52 (39) (2013) 14019–14029, https://doi.org/10.1021/ie401308v.

[17] W. Li, Q. He, C. Pei, B. Hou, Experimental and theoretical investigation of the adsorption behaviour of new triazole derivatives as inhibitors for mild steel corrosion in acid media, Electrochim. Acta 52 (22) (2007) 6386–6394, https://doi.org/10.1016/j.electacta.2007.04.077.

[18] A.Y. Musa, R.T.T. Jalgham, A.B. Mohamad, Molecular dynamic and quantum chemical calculations for phthalazine derivatives as corrosion inhibitors of mild steel in 1 M HCl, Corros. Sci. 56 (2012) 176–183, https://doi.org/10.1016/j.corsci.2011.12.005.

[19] A.Y. Musa, A.A.H. Kadhum, A.B. Mohamad, M.S. Takriff, Molecular dynamics and quantum chemical calculation studies on 4,4-dimethyl-3-thiosemicarbazide as corrosion inhibitor in 2.5 M H_2SO_4, Mater. Chem. Phys. 129 (1–2) (2011) 660–665, https://doi.org/10.1016/j.matchemphys.2011.05.010.

[20] A.Y. Musa, A.A.H. Kadhum, A.B. Mohamad, M.S. Takriff, Experimental and theoretical study on the inhibition performance of triazole compounds for mild steel corrosion, Corros. Sci. 52 (10) (2010) 3331–3340, https://doi.org/10.1016/j.corsci.2010.06.002.

[21] P.M. Niamien, F.K. Essy, A. Trokourey, A. Yapi, H.K. Aka, D. Diabate, Correlation between the molecular structure and the inhibiting effect of some benzimidazole derivatives, Mater. Chem. Phys. 136 (1) (2012) 59–65, https://doi.org/10.1016/j.matchemphys.2012.06.025.

[22] N.O. Obi-Egbedi, I.B. Obot, S.A. Umoren, Spondias mombin L. as a green corrosion inhibitor for aluminium in sulphuric acid: Correlation between inhibitive effect

[21] The free energy of a water vapor is:

$$G_{\text{vapor}}^{(\text{g})} = G^{1\text{atm,(g)}} + RT \ln \frac{p_{\text{vapor}}}{1\ \text{atm}},$$

whereas the free energy of a liquid water is given by Eq. (A.16), i.e.:

$$G^{(l)} = G^{1\text{atm,(g)}} + RT \ln \frac{55.34\ \text{M}}{\text{“1atm”}} + G_{\text{solv}}.$$

By utilizing the $G^{(\text{g})} = G^{(\text{l})}$ relation and canceling the $G^{1\text{atm,(g)}}$ term on both sides, one obtains:

$$RT \ln \frac{p_{\text{vapor}}}{1\ \text{atm}} = RT \ln \frac{55.34\ \text{M}}{\text{“1atm”}} + G_{\text{solv}}(\text{H}_2\text{O})$$

Hence:

$$G_{\text{solv}}(\text{H}_2\text{O}) = RT \ln \frac{p_{\text{vapor}}}{1\ \text{atm}} - RT \ln \frac{55.34\ \text{M}}{\text{“1atm”}} = -9 - 18\ \text{kJ/mol} = -27\ \text{kJ/mol},$$

where the value of 0.0313 atm was used for p_{vapor}.

and electronic properties of extracts major constituents using density functional theory, Arab. J. Chem. 5 (3) (2012) 361–373, https://doi.org/10.1016/j.arabjc.2010.09.002.
[23] N. Obi-Egbedi, I. Obot, Adsorption behavior and corrosion inhibitive potential of xanthene on mild steel/sulphuric acid interface, Arabian J. Chem. 5 (1) (2012) 121–133, https://doi.org/10.1016/j.arabjc.2010.08.004.
[24] M.K. Pavithra, T.V. Venkatesha, M.K.P. Kumar, H.C. Tondan, Inhibition of mild steel corrosion by rabeprazole sulfide, Corros. Sci. 60 (2012) 104–111, https://doi.org/10.1016/j.corsci.2012.04.003.
[25] D.K. Yadav, M.A. Quraishi, B. Maiti, Inhibition effect of some benzylidenes on mild steel in 1 M HCl: An experimental and theoretical correlation, Corros. Sci. 55 (2012) 254–266, https://doi.org/10.1016/j.corsci.2011.10.030.
[26] M. Yadav, S. Kumar, Experimental, thermodynamic and quantum chemical studies on adsorption and corrosion inhibition performance of synthesized pyridine derivatives on N80 steel in HCl solution, Surf. Interface Anal. 46 (4) (2014) 254–268, https://doi.org/10.1002/sia.5408.
[27] A. Ongun Yüce, B. Dogru Mert, G. Kardaş, B. Yazıcı, Electrochemical and quantum chemical studies of 2-amino-4-methyl-thiazole as corrosion inhibitor for mild steel in HCl solution, Corros. Sci. 83 (2014) 310–316, https://doi.org/10.1016/j.corsci.2014.02.029.
[28] G. Moretti, F. Guidi, G. Grion, Tryptamine as a green iron corrosion inhibitor in 0.5 M deaerated sulphuric acid, Corros. Sci. 46 (2) (2004) 387–403, https://doi.org/10.1016/S0010-938X(03)00150-1.
[29] F.M. Donahue, K. Nobe, Theory of organic corrosion inhibitors: Adsorption and linear free energy relationships, J. Electrochem. Soc. 112 (9) (1965) 886–891, https://doi.org/10.1149/1.2423723.
[30] E. Khamis, F. Bellucci, R.M. Latanision, E.S.H. El-Ashry, Acid corrosion inhibition of nickel by 2-(triphenosphoranylidene) succinic anhydride, Corrosion 47 (9) (1991) 677–686, https://doi.org/10.5006/1.3585307.
[31] A. Kokalj, Molecular modeling of organic corrosion inhibitors: calculations, pitfalls, and conceptualization of molecule-surface bonding, Corros. Sci. 193 (2021), 109650, https://doi.org/10.1016/j.corsci.2021.109650.
[32] M.S. Walczak, P. Morales-Gil, R. Lindsay, Determining Gibbs energies of adsorption from corrosion inhibition efficiencies: Is it a reliable approach? Corros. Sci. 155 (2019) 182–185, https://doi.org/10.1016/j.corsci.2019.04.040.
[33] S. Ghareba, S. Omanovic, Interaction of 12-aminododecanoic acid with a carbon steel surface: Towards the development of 'green' corrosion inhibitors, Corros. Sci. 52 (6) (2010) 2104–2113, https://doi.org/10.1016/j.corsci.2010.02.019.
[34] F. Schreiber, Structure and growth of self-assembling monolayers, Prog. Surf. Sci. 65 (5) (2000) 151–257, https://doi.org/10.1016/S0079-6816(00)00024-1.
[35] S.M. Wetterer, D.J. Lavrich, T. Cummings, S.L. Bernasek, G. Scoles, Energetics and kinetics of the physisorption of hydrocarbons on Au(111), J. Phys. Chem. B 102 (46) (1998) 9266–9275, https://doi.org/10.1021/jp982338.
[36] D.J. Lavrich, S.M. Wetterer, S.L. Bernasek, G. Scoles, Physisorption and chemisorption of alkanethiols and alkyl sulfides on Au(111), J. Phys. Chem. B 102 (18) (1998) 3456–3465, https://doi.org/10.1021/jp980047v.
[37] W. Durnie, R. De Marco, A. Jefferson, B. Kinsella, Deveopment of a structure-activity relationship for oil field corrosion inhibitors, J. Electrochem. Soc. 146 (5) (1999) 1751–1756, https://doi.org/10.1149/1.1391837.
[38] X. Shi, R.Q. Zhang, C. Minot, K. Hermann, M.A. Van Hove, W. Wang, N. Lin, Complex molecules on a flat metal surface: Large distortions induced by chemisorption can make physisorption energetically more favorable, J. Phys. Chem. Lett. 1 (19) (2010) 2974–2979, https://doi.org/10.1021/jz1011753.
[39] A.D. McNaught, A. Wilkinson (Eds.), IUPAC Compendium of Chemical Terminology (the "Gold Book"), 2nd Edition, Blackwell Scientific Publications, Oxford, 1997, https://doi.org/10.1351/goldbook.
[40] S.J. Chalk, Chemisorption (chemical adsorption), IUPAC Gold Book (2019), https://doi.org/10.1351/goldbook.C01048.
[41] S.J. Chalk, Physisorption (physical adsorption), IUPAC Gold Book (2019), https://doi.org/10.1351/goldbook.P04667.
[42] Contributors to Wikimedia projects, Physisorption – Wikipedia, [Online; accessed 14. Jul. 2021] (2021). ⟨https://en.wikipedia.org/w/index.php?title=Physisorption&oldid=1028742416⟩.
[43] A. Kokalj, S. Peljhan, Density functional theory study of ATA, BTAH, and BTAOH as copper corrosion inhibitors: Adsorption onto Cu(111) from gas phase, Langmuir 26 (18) (2010) 14582–14593, https://doi.org/10.1021/la1019789.
[44] A. Kokalj, S. Peljhan, M. Finšgar, I. Milošev, What determines the inhibition effectiveness of ATA, BTAH, and BTAOH corrosion inhibitors on copper? J. Am. Chem. Soc. 132 (46) (2010) 16657–16668, https://doi.org/10.1021/ja107704y.
[45] S. Peljhan, A. Kokalj, DFT study of gas-phase adsorption of benzotriazole on Cu (111), Cu(100), Cu(110), and low coordinated defects thereon, Phys. Chem. Chem. Phys. 13 (2011) 20408–20417, https://doi.org/10.1039/C1CP21873E.
[46] A. Kokalj, N. Kovačević, S. Peljhan, M. Finšgar, A. Lesar, I. Milošev, Triazole, benzotriazole, and naphthotriazole as copper corrosion inhibitors: I. Molecular electronic and adsorption properties, ChemPhysChem 12 (18) (2011) 3547–3555, https://doi.org/10.1002/cphc.201100537.
[47] N. Kovačević, A. Kokalj, Chemistry of the interaction between azole type corrosion inhibitor molecules and metal surfaces, Mater. Chem. Phys. 137 (1) (2012) 331–339, https://doi.org/10.1016/j.matchemphys.2012.09.030.
[48] B. Cordero, V. Gómez, A.E. Platero-Prats, M. Revés, J. Echeverría, E. Cremades, F. Barragán, S. Alvarez, Covalent radii revisited, Dalton Trans. (21) (2008) 2832–2838, https://doi.org/10.1039/B801115J.
[49] A. Bondi, van der Waals volumes and radii, J. Phys. Chem. 68 (3) (1964) 441–451, https://doi.org/10.1021/j100785a001.
[50] M. Poberžnik, D. Costa, A. Hemeryck, A. Kokalj, Insight into the bonding of silanols to oxidized aluminum surfaces, J. Phys. Chem. C 122 (17) (2018) 9417–9431, https://doi.org/10.1021/acs.jpcc.7b12552.
[51] M. Poberžnik, A. Kokalj, Implausibility of bidentate bonding of the silanol headgroup to oxidized aluminum surfaces, Appl. Surf. Sci. 492 (2019) 909–918, https://doi.org/10.1016/j.apsusc.2019.04.032.
[52] M. Poberžnik, Quantum mechanical modeling of the oxidation of aluminum surfaces and their interactions with corrosion inhibitors: doctoral dissertation, Ph. D. thesis, Faculty of Chemistry and Chemical Technology, University of Ljubljana, Ljubljana (2019).
[53] M.R. Alexander, G.E. Thompson, G. Beamson, Characterization of the oxide/hydroxide surface of aluminium using x-ray photoelectron spectroscopy: a procedure for curve fitting the O 1s core level, Surf. Interface Anal. 29 (7) (2000) 468–477, https://doi.org/10.1002/1096-9918(200007)29:7<468::AID-SIA890>3.0.CO;2-V.
[54] B.C. Bunker, G.C. Nelson, K.R. Zavadil, J.C. Barbour, F.D. Wall, J.P. Sullivan, C. F. Windisch, M.H. Engelhardt, D.R. Baer, Hydration of passive oxide films on aluminum, J. Phys. Chem. B 106 (18) (2002) 4705–4713, https://doi.org/10.1021/jp013246e.
[55] M. Poberžnik, F. Chiter, I. Milošev, P. Marcus, D. Costa, A. Kokalj, DFT study of *n*-alkyl carboxylic acids on oxidized aluminum surfaces: from standalone molecules to self-assembled-monolayers, Appl. Surf. Sci. 525 (2020), 146156, https://doi.org/10.1016/j.apsusc.2020.146156.
[56] M. Corral Valero, B. Prelot, G. Lefévre, MUSIC speciation of γ-Al_2O_3 at the solid liquid interface: How DFT calculations can help with amorphous and poorly crystalline materials, Langmuir 35 (40) (2019) 12986–12992, https://doi.org/10.1021/acs.langmuir.9b02788.
[57] A. Motta, M.-P. Gaigeot, D. Costa, Ab initio molecular dynamics study of the AlOOH boehmite/water interface: Role of steps in interfacial Grotthus proton transfers, J. Phys. Chem. C 116 (23) (2012) 12514–12524, https://doi.org/10.1021/jp3000812.
[58] V.P. Zhdanov, J. Pavlíček, Z. Knor, Preexponential factors for elementary surface processes, Catal. Rev.: Sci. Eng. 30 (4) (1988) 501–517, https://doi.org/10.1080/01614948808071752.
[59] V. Zhdanov, Arrhenius parameters for rate processes on solid surfaces, Surf. Sci. Rep. 12 (5) (1991) 185–242, https://doi.org/10.1016/0167-5729(91)90011-L.
[60] A. Migani, F. Illas, A systematic study of the structure and bonding of halogens on low-index transition metal surfaces, J. Phys. Chem. B 110 (24) (2006) 11894–11906, https://doi.org/10.1021/jp060400u.
[61] S. Peljhan, A. Kokalj, Adsorption of chlorine on Cu(111): A density-functional theory study, J. Phys. Chem. C 113 (32) (2009) 14363–14376, https://doi.org/10.1021/jp902273k.
[62] A. Kokalj, On the HSAB based estimate of charge transfer between adsorbates and metal surfaces, Chem. Phys. 393 (2012) 1–12, https://doi.org/10.1016/j.chemphys.2011.10.021.
[63] The argument that a too strong molecule–surface interaction weakens the neighboring metal–metal bonds was introduced to the author by Vincent Maurice during author's talk given at Research Group of Physical Chemistry of Surfaces, Institut de Recherche de Chimie, Paris, (22 November 2015)
[64] P. Marcus, V. Maurice, H.-H. Strehblow, Localized corrosion (pitting): A model of passivity breakdown including the role of the oxide layer nanostructure, Corros. Sci. 50 (9) (2008) 2698–2704, https://doi.org/10.1016/j.corsci.2008.06.047.
[65] F.B. Growcock, W.W. Frenier, P.A. Andreozzi, Inhibition of steel corrosion in HCl by derivatives of cinnamaldehyde: Part II. Structure-activity correlations, Corrosion 45 (12) (1989) 1007–1015, https://doi.org/10.5006/1.3585008.
[66] I. Lukovits, E. Kálmán, F. Zucchi, Corrosion inhibitors-correlation between electronic structure and efficiency, Corrosion 57 (1) (2001) 3–8, https://doi.org/10.5006/1.3290328.
[67] A. Kokalj, On the alleged importance of the molecular electron-donating ability and the HOMO-LUMO gap in corrosion inhibition studies, Corros. Sci. 180 (2021), 109016, https://doi.org/10.1016/j.corsci.2020.109016.
[68] J.P. Perdew, K. Burke, M. Ernzerhof, Generalized gradient approximation made simple, Phys. Rev. Lett. 77 (18) (1996) 3865–3868, https://doi.org/10.1103/PhysRevLett.77.3865.
[69] D. Vanderbilt, Soft self-consistent pseudopotentials in a generalized eigenvalue formalism, Phys. Rev. B 41 (1990) 7892–7895, https://doi.org/10.1103/PhysRevB.41.7892.
[70] Ultrasoft pseudopotentials for H, C, N, O, Al, Si, Fe, and Cu atoms were taken from the Quantum Espresso Pseudopotential Download Page at http://www.quantum-espresso.org/pseudopotentials (files: H.pbe-rrkjus.UPF, C.pbe-rrkjus.UPF, N.pbe-rrkjus.UPF, O.pbe-rrkjus.UPF, Al.pbe-n-rrkjus_psl.0.1.UPF, Si.pbe-n-rrkjus_psl.0.1.UPF, Fe.pbe-sp-van.UPF, and Cu.pbe-d-rrkjus.UPF). (2021).
[71] P. Giannozzi, S. Baroni, N. Bonini, M. Calandra, R. Car, C. Cavazzoni, D. Ceresoli, G.L. Chiarotti, M. Cococcioni, I. Dabo, A. DalCorso, S. de Gironcoli, S. Fabris, G. Fratesi, R. Gebauer, U. Gerstmann, C. Gougoussis, A. Kokalj, M. Lazzeri, G. Martin-Samos, N. Marzari, F. Mauri, R. Mazzarello, S. Paolini, A. Pasquarello, L. Paulatto, C. Sbraccia, S. Scandolo, G. Sclauzero, A.P. Seitsonen, A. Smogunov, P. Umari, R.M. Wentzcovitch, Quantum ESPRESSO: a modular and open-source software project for quantum simulations of materials, J. Phys: Condens. Matter 21 (39) (2009), 395502, https://doi.org/10.1088/0953-8984/21/39/395502 code available from, ⟨http://www.quantum-espresso.org/⟩.
[72] P. Giannozzi, O. Andreussi, T. Brumme, O. Bunau, M.B. Nardelli, M. Calandra, R. Car, C. Cavazzoni, D. Ceresoli, M. Cococcioni, N. Colonna, I. Carnimeo, A. D. Corso, S. de Gironcoli, P. Delugas, R. DiStasio, A. Ferretti, A. Floris, G. Fratesi, G. Fugallo, R. Gebauer, U. Gerstmann, F. Giustino, T. Gorni, J. Jia, M. Kawamura, H.-Y. Ko, A. Kokalj, E. Küçübenli, M. Lazzeri, M. Marsili, N. Marzari, F. Mauri, N.

L. Nguyen, H.-V. Nguyen, A.O. de-la Roza, L. Paulatto, S. Poncé, D. Rocca, R. Sabatini, B. Santra, M. Schlipf, A.P. Seitsonen, A. Smogunov, I. Timrov, T. Thonhauser, P. Umari, N. Vast, X. Wu, S. Baroni, Advanced capabilities for materials modelling with QUANTUM espresso, J. Phys: Condens. Matter 29 (2017), 465901, https://doi.org/10.1088/1361-648X/aa8f79.

[73] H.J. Monkhorst, J.D. Pack, Special points for Brillouin-zone integrations, Phys. Rev. B 13 (12) (1976) 5188–5192, https://doi.org/10.1103/PhysRevB.13.5188.

[74] M. Methfessel, A.T. Paxton, High-precision sampling for Brillouin-zone integration in metals, Phys. Rev. B 40 (1989) 3616–3621, https://doi.org/10.1103/PhysRevB.40.3616.

[75] S. Grimme, Semiempirical GGA-type density functional constructed with a long-range dispersion correction, J. Comput. Chem. 27 (15) (2006) 1787–1799, https://doi.org/10.1002/jcc.20495.

[76] S. Baroni, S. de Gironcoli, A. DalCorso, P. Giannozzi, Phonons and related crystal properties from density-functional perturbation theory, Rev. Mod. Phys. 73 (2001) 515–562, https://doi.org/10.1103/RevModPhys.73.515.

[77] R.F. Ribeiro, A.V. Marenich, C.J. Cramer, D.G. Truhlar, Use of solution-phase vibrational frequencies in continuum models for the free energy of solvation, J. Phys. Chem. B 115 (49) (2011) 14556–14562, https://doi.org/10.1021/jp205508z.

[78] O. Andreussi, I. Dabo, N. Marzari, Revised self-consistent continuum solvation in electronic-structure calculations, J. Chem. Phys. 136 (6) (2012), 064102, https://doi.org/10.1063/1.3676407.

[79] G. Fisicaro, L. Genovese, O. Andreussi, S. Mandal, N.N. Nair, N. Marzari, S. Goedecker, Soft-sphere continuum solvation in electronic-structure calculations, J. Chem. Theory Comput. 13 (8) (2017) 3829–3845, https://doi.org/10.1021/acs.jctc.7b00375.

[80] G. Henkelman, H. Jónsson, Improved tangent estimate in the nudged elastic band method for finding minimum energy paths and saddle points, J. Chem. Phys. 113 (22) (2000) 9978–9985, https://doi.org/10.1063/1.1323224.

[81] G. Henkelman, B.P. Uberuaga, H. J'onsson, A climbing image nudged elastic band method for finding saddle points and minimum energy paths, J. Chem. Phys. 113 (22) (2000) 9901–9904, https://doi.org/10.1063/1.1329672.

[82] W. Schmickler, E. Santos. Interfacial electrochemistry, 2nd Edition, Springer Science & Business Media, Verlag Berlin Heidelberg, 2010.

[83] V.S. Bryantsev, M.S. Diallo, W.A. Goddard III, Calculation of solvation free energies of charged solutes using mixed cluster/continuum models, J. Phys. Chem. B 112 (32) (2008) 9709–9719, https://doi.org/10.1021/jp802665d.

[84] D.R. Lide (Ed.), CRC Handbook of Chemistry and Physics, 85th Edition, CRC Press, Boca Raton, Florida USA, 2005.